

UC Davis

UC Davis Previously Published Works

Title

Reflective afocal adaptive optics: optical coherence tomography retinal imaging system

Permalink

<https://escholarship.org/uc/item/2q48q8zx>

ISBN

9780819493361

Authors

Lee, Sang Hyuck
Werner, John S
Zawadzki, Robert J

Publication Date

2013-03-26

DOI

10.1117/12.2003421

Peer reviewed

Reflective Afocal Adaptive Optics - Optical Coherence Tomography Retinal Imaging System

Sang Hyuck Lee, John S. Werner and Robert J. Zawadzki*

Vision Science and Advanced Retinal Imaging Laboratory (VSRI) and Dept. of Ophthalmology & Vision Science, UC Davis, 4860 Y Street, Suite 2400, Sacramento, CA USA 95817

ABSTRACTS

We present a new design for a reflective afocal AO-OCT retinal imaging system. The optical performance of this instrument is compared to our previous multimodal AO-OCT/AO-SLO retinal imaging system. The feasibility of new instrumentation for improved visualization of microscopic retinal structures will be discussed. Examples of images acquired with this new AO-OCT instrument will be presented.

Keywords: optical coherence tomography; ophthalmology; imaging system; medical optics instrumentation

1. INTRODUCTION

Over the last decade, development of adaptive optics (AO) retinal imaging instruments made possible routine imaging of in vivo human retina at the cellular scale. However, the first reports of in-vivo imaging of foveal cones and the rod photoreceptor mosaic have only recently been published. One of the reasons for achieving improved performance and resolution of AO systems can be attributed to aberration-free design of AO imaging instruments. We previously described a system combining AO-SLO with AO-OCT that uses “in plane” optical design of the AO-OCT sample arm [1]. Here we present progress on developing the next generation of adaptive optics systems that implements an aberration-free and pupil wander free design using reflective optics. A similar design strategy has been recently implemented in AO-SLO systems for retinal imaging [2,3].

2. MATERIALS AND METHODS

2.1 Optical design

Figure 1 shows screenshots of the 3D layout of the imaging optics of the AO-OCT sample arm as visualized by optical design software (Zemax). Similar to our original design, we used a cascade of focal telescopes (created by pairs of spherical mirrors) to produce conjugate planes of the eye pupil with all key optical components, including X and Y scanning mirrors, wavefront correctors and a Hartmann-Shack (H-S) wavefront sensor.

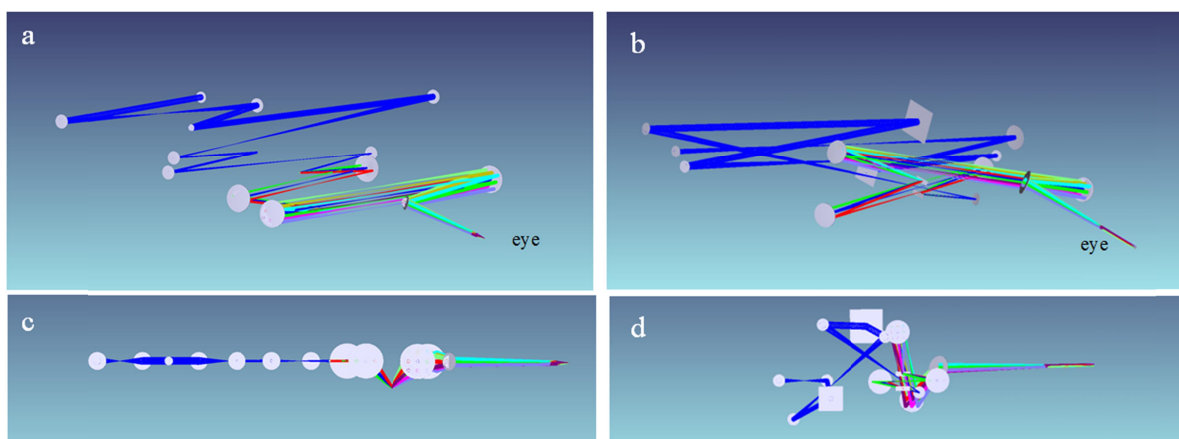


Figure 1. 3D visualization of old (left) and new (right) afocal AO-OCT sample arm design. Angle view of old (a) and new (b) AO-OCT sample arm. Side view of old (c) and new (d) AO-OCT sample arm.

*rjzawadzki@ucdavis.edu;

phone 1 916 734-5839;

fax 1 916 734-5839;

<http://vsri.ucdavis.edu/>

The main difference from our prior system is that the current design places optical elements out of the single plane in order to minimize system residual aberration. Using optical design software we found that optical aberrations of imaging systems are responsible for reducing performance of adaptive optics. Therefore, implementation of aberration-free design of optical system is critical for achieving optimum performance of AO system and for measuring and correcting aberration of the sample, in our case the subject's ocular aberrations. As shown in Fig. 1(a), (c), and Fig. 2 (a), the spherical mirrors are placed in regular order in old AO-OCT sample arm. Inevitably, the astigmatism is cumulated as the number of mirrors is increased. The key idea of the new AO-OCT sample arm design is to counterbalance the astigmatism by changing the order of mirrors that are placed in the sample arm not only in one plane but also 'out of the plane' as shown in Fig. 1(b), (d), and Fig 2 (b). The aberrations are counterbalanced at each corresponding mirror that generates the opposite direction of light. This principle of design was well maintained during the optical design and worked very well.

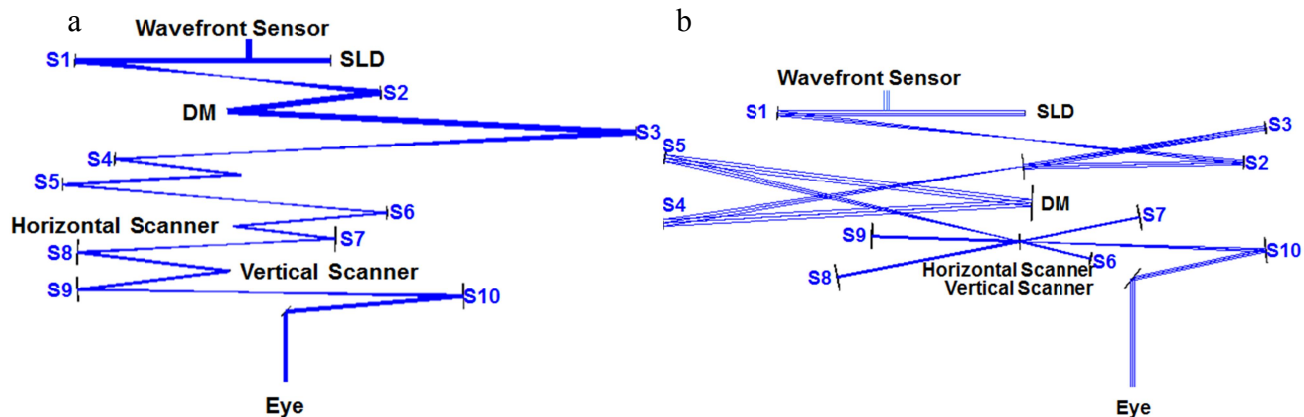


Figure 2. Top view of old (a) and new (b) AO-OCT sample arm. DM – Deformable mirror; SLD – Superluminescent Diode; S1-S10: Spherical mirrors.

Figure 3 shows spot diagrams of the old and new AO-OCT sample arm plotted as a function of scanning position ($3^\circ \times 3^\circ$). In the prior AO-OCT design, the main aberration remaining was astigmatism. Off-axis aberration, like astigmatism, is severe in a cascaded telescope system because it is always cumulated as light goes through all the mirrors that are placed sequentially in a single plane. In our new AO-OCT design, geometrical spot size is suppressed under the size of the Airy Disk through the new concept of design.

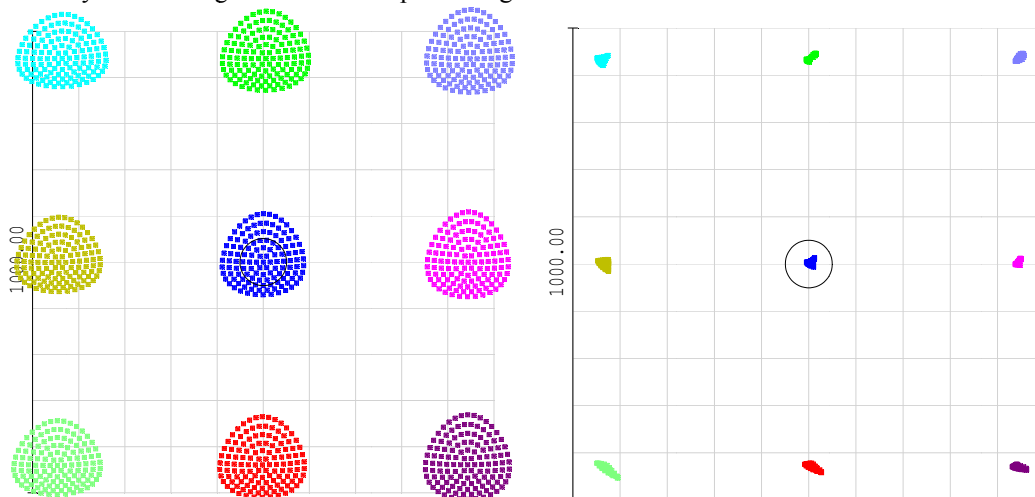


Figure 3. Comparison of spot diagram with Airy Disk (Black circle) as a function of scanner position over $3^\circ \times 3^\circ$ field for old (left) and new (right) design. (Spot diagrams are magnified by 20 times.)

Figure 4 shows a comparison of root mean square (RMS) wavefront error of the old and new AO-OCT sample arm plotted as a function of scanning position ($3^\circ \times 3^\circ$). The initial wavefront aberration of our new system for $3^\circ \times 3^\circ$ FOV is suppressed under 10nm. The old system had larger initial wavefront aberration, 230nm. Reduction of residual RMS of the system allows the entire correcting stroke of the wavefront corrector to be used for improving aberrations of the subject's eye rather than the system itself.

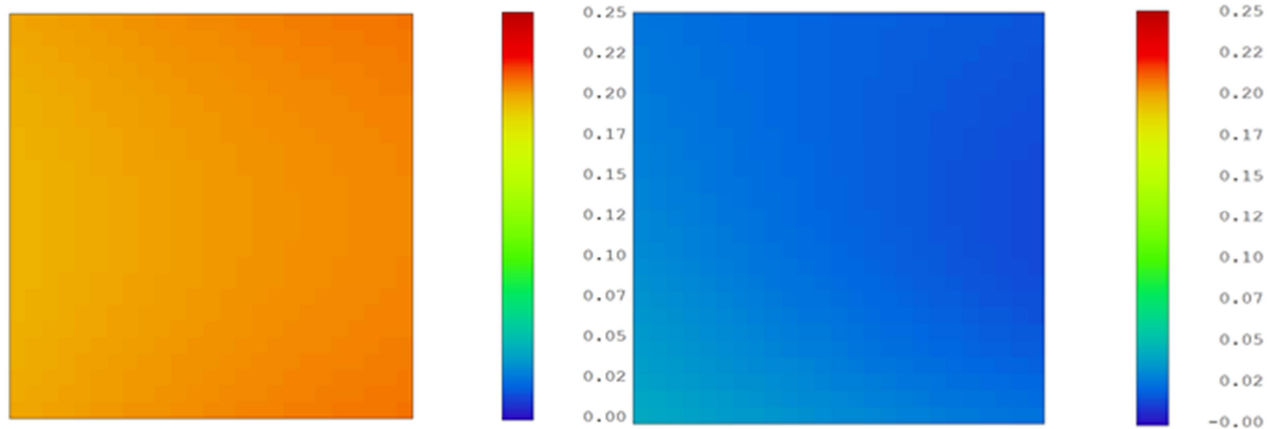


Figure 4. Comparison of RMS wavefront error as a function of scanner position for old (left) and new (right) design.

Another important benefit of our new optical design is reduction of pupil wander observed at the system entrance pupil plane during imaging. Minimizing this effect is critical for proper measurements and correction of wavefront error. Figure 5 shows the comparison of pupil wander for the old and new AO-OCT sample arm design plotted as a function of scanning position ($3^\circ \times 3^\circ$). The maximum pupil wander of our new system for $3^\circ \times 3^\circ$ FOV is under 0.1mm which is also lower than the value of the previous system, 0.43mm.

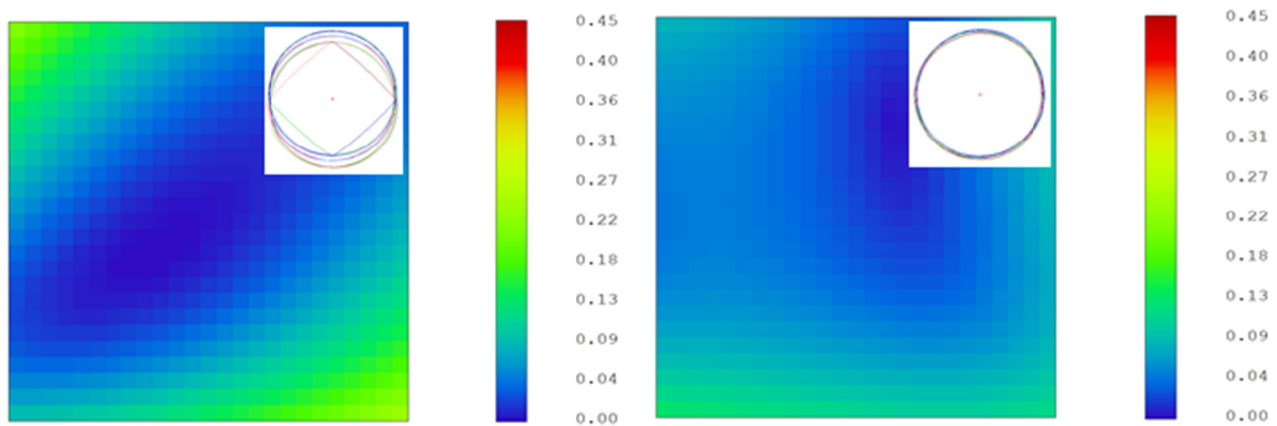


Figure 5. Comparisons of pupil wander as a function of imaging beam position (scanning angle) of old (left) and new (right) AO-OCT design. The top right corner of each panel shows a plot of the instrument's pupil as observed at the eye's pupil for several scanning angles.

Pupil wander has impairs performance of an AO system. In our system exposure time of the wavefront sensor is on the order of 30-50ms; thus, different parts of the eye pupil are sampled during single wavefront data acquisition, which "blurs" measured wavefronts. This can also result in creation of periodic modulations of measured wavefront as different parts of the pupil have different wavefronts. To reduce this effect we use identical "frame rates" of AO and imaging system.

2.2 Experimental system

Figure 6 shows the experimental setup of the new AO-OCT sample arm. In the optical design, we used a series of focal telescopes to image the eye's pupil on all key optical components, including vertical and horizontal scanning mirrors, wavefront corrector (deformable mirror, DM), the Hartmann-Shack wavefront sensor and the fiber collimator for light delivery. Superluminescent Diode (SLD, T840-HP) is used as a source. The center wavelength was 840nm and the bandwidth was 112nm with output power of 16mW. Light from a superluminescent diode is split by a 90/10 fiber directional coupler into the reference and sample arms of the OCT system's Michelson interferometer, respectively.

The OCT acquisition engine is similar to the one we previously published in the paper describing our phase variance OCT instrument [4]. Light back-scattered from the retina is combined with light from the reference arm and the spectral fringes are acquired in the detection channel of the OCT spectrometer. A water cuvette placed in the reference arm approximately matches the chromatic dispersion induced by the human eye in the sample arm; any remaining dispersion mismatch is corrected by Fourier-domain OCT reconstruction software [5]. Each solid and dotted line represents the direction of the light. Light goes up and down to minimize the aberration of the system and the pupil wander at the eye plane. In our old AO-OCT system, the aberrations were cumulated as light goes through all the mirrors because it was designed in a single plane. The new AO-OCT system is not designed in a single plane and the aberrations are counterbalanced at each corresponding mirror that generates the opposite direction of light.

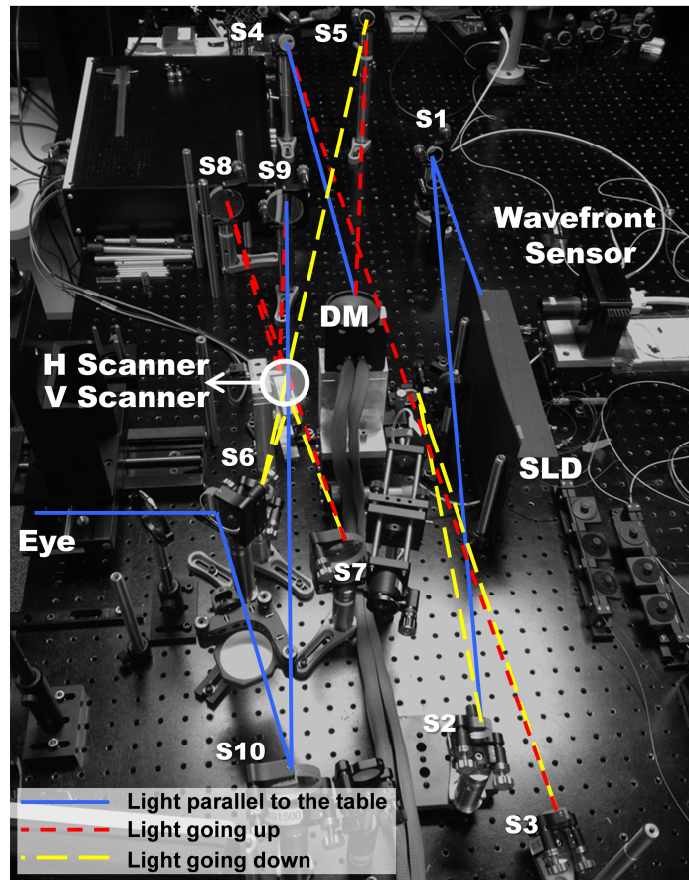


Figure 6. Experimental setup of new afocal AO-OCT sample arm

3. RESULTS

3.1 Wavefront correction by deformable mirror

The residual system aberrations are corrected in software by the deformable mirror (DM). To quantify the correction and maximum stroke of the DM, we generated defocus errors on the eye pupil. Defocus values from -4 to +4 Diopter (Dpt)

are applied and corrected by the DM. This corresponds to evaluating performance of our system for imaging patients with different refractive error. The wavefront sensor measures the residual system aberrations for DM correction. Figure 7 shows the RMS wavefront error of the OCT system when the defocus is applied (dotted line) and corrected (bold line). The results demonstrate that the new AO-OCT system can achieve diffraction-limited performance for all the defocus generated with DM correction. The RMS wavefront errors were under 30nm which is much lower than the diffraction limit, 65nm.

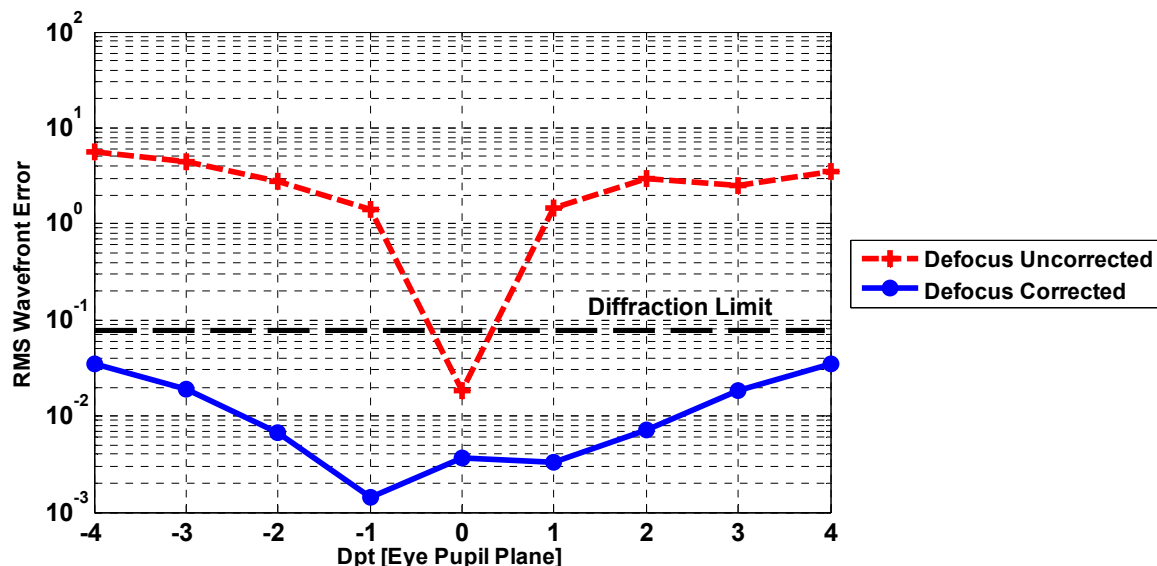


Figure 7. RMS wavefront error of OCT system for each defocuses and corrections by DM (Log scale)

Figure 8 shows simulated shapes of the Deformable mirror during correction of defocus present at the entrance pupil. The maximum DM stroke needed to correct ± 4 Dpt defocus was $\pm 9.2\mu\text{m}$, below the deformation range of the Alpaio mirror ($\pm 22\mu\text{m}$) used in our system.

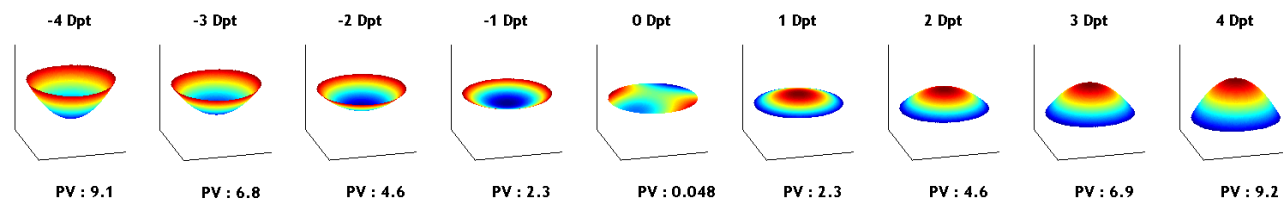


Figure 8. DM Strokes (μm) for each defocus value.

3.2 In-vivo imaging of the retina

Figure 9 shows each layer of retina from two volumetric scans which have different focal positions of scanning beams. The volume data were acquired at the same position from the normal subject. Optical power on the cornea was $250\mu\text{W}$ and the scanning speed was 82.5 kHz with $0.75^\circ \times 0.75^\circ$ FOV. Due to the large pupil size and short focal depth, we could separate adjacent layers clearly from the volume data. Images of en-face projection views of photoreceptor layers extracted from volumetric scans show improved resolution and contrast compared to our previous AO-OCT system.

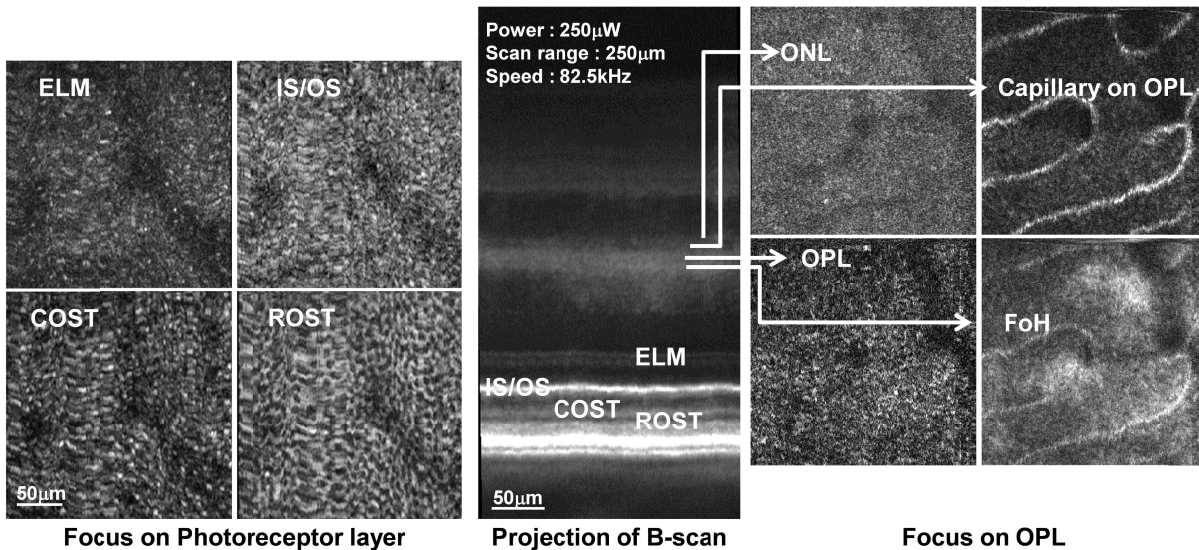


Figure 9. Images from two volumetric scans (beam focal position is moved from photoreceptor layer to OPL for better resolution.). ELM – external limiting membrane; IS/OS – photoreceptors inner /outer segment junction, COST – cone outer segments tips; ROST rods outer segments tips, ONL – outer nuclear layer, OPL – outer plexiform layer, FoH – fibers of Henle.

4. CONCLUSIONS

An off-axis AO-OCT system was designed and successfully implemented allowing minimization of the wavefront error and pupil wander to result in better resolution and retinal image quality. Counterbalancing of wavefront errors and minimizing pupil wander was possible using conventional cascade of focal telescopes by placing the telescopes non-sequentially. Increased lateral resolution allowed visualization of 3D morphology of cone and rod photoreceptors mosaics.

5. ACKNOWLEDGMENTS

We gratefully acknowledge the contributions of VSRI UC Davis lab members. This research was supported by the National Eye Institute (EY 014743) and Research to Prevent Blindness (RPB).

REFERENCES

- [1] Zawadzki, R. J., Jones, S. M., Pilli, S., Balderas-Mata, S., Kim, D. Y., Olivier, S. S., & Werner, J. S., "Integrated adaptive optics optical coherence tomography and adaptive optics scanning laser ophthalmoscope system for simultaneous cellular resolution in vivo retinal imaging," *Biomedical optics express*, 2(6), 1674-1686 (2011).
- [2] Dubra, A., & Sulai, Y., "Reflective afocal broadband adaptive optics scanning ophthalmoscope," *Biomedical Optics Express* 2(6), 1757 (2011).
- [3] Merino, D., Duncan, J.L., Tiruveedhula, P., Roorda, A., "Observation of cone and rod photoreceptors in normal subjects and patients using a new generation Adaptive Optics Scanning Laser Ophthalmoscope" *Biomedical Optics Express*, 2(8), 2189-2201 (2011).
- [4] Kim, D. Y., Fingler, J., Werner, J. S., Schwartz, D. M., Fraser, S. E., & Zawadzki, R. J. "In vivo volumetric imaging of human retinal circulation with phase-variance optical coherence tomography," *Biomedical optics express* 2(6), 1504-1513 (2011).
- [5] Zawadzki, R. J., Jones, S. M., Olivier, S. S., Zhao, M., Bower, B. A., Izatt, J. A., Olivier, S. S., & Werner, J. S., "Adaptive-optics optical coherence tomography for high-resolution and high-speed 3D retinal in vivo imaging," *Optics express* 13(21), 8532 (2005).